Reaction Chemistry & Engineering

Linking fundamental chemistry and engineering to create scalable, efficient processes

Accepted Manuscript

This article can be cited before page numbers have been issued, to do this please use: V. Cool, S. Riaño, T. Van Gerven and K. Binnemans, *React. Chem. Eng.*, 2026, DOI: 10.1039/D5RE00536A.

ROYAL SOCIETY OF CHEMISTRY

rsc.li/reaction-engineering

Manuscript for: Reaction Chemistry & Engineering

View Article Online
DOI: 10.1039/D5RE00536A

Characterization and purification of the ionic liquid Cyphos IL 101 by non-aqueous solvent extraction

Vincent Cool[†], Sofia Riaño[†], Tom Van Gerven[‡], Koen Binnemans[†]*

[†] KU Leuven, Department of Chemistry, Celestijnenlaan 200F, P.O. box 2404, B-3001 Leuven, Belgium.

[‡] KU Leuven, Department of Chemical Engineering, Celestijnenlaan 200F, P.O. Box 2424, B-3001 Leuven, Belgium.

*Corresponding author:

Email: Koen.Binnemans@kuleuven.be

View Article Online
DOI: 10.1039/D5RE00536A

Abstract

The chemical composition of the quaternary phosphonium ionic liquid Cyphos IL 101 was characterized by ^{31}P NMR spectroscopy and LC–MS analysis, revealing the presence of at least 22 distinct phosphorus-containing species in the commercial product. Anomalous results observed when using deuterated chloroform as a solvent for NMR analysis of Cyphos IL 101 were addressed, demonstrating that protic solvents are essential for accurate quantitative NMR measurements. Different batches of Cyphos IL 101 showed significant variations in the concentrations of trialkylphosphonium chlorides and trialkylphosphane oxides. Aging and storage conditions were identified as key factors influencing the overall composition of the ionic liquid. A purification strategy for Cyphos IL 101 based on non-aqueous solvent extraction using ethylene glycol with NaCl was developed. A purity of 99% was obtained by a process with 10 steps. Quantitative removal of the protonated phosphanes was achieved, but the overall purity remained dependent on the initial composition, particularly due to the poor extractability of the phosphane oxides. Process kinetics and settling behavior were investigated, and the method was successfully demonstrated on a liter scale in continuous countercurrent mode in a Kühni column with rotary agitation, achieving the same 99% purity as in batch operations. The variation in Cyphos IL 101's composition across batches and within batches over time might have serious implications for the usefulness of this ionic liquid as an extractant for metal ions.

Keywords: Extraction column; ionic liquids; liquid-liquid extraction; non-aqueous solvent extraction; quantitative NMR; solvent extraction.

View Article Online
DOI: 10.1039/D5RE00536A

Introduction

Ionic liquids (ILs) are solvents that consist entirely of ions and that are liquid at or near room temperature. They have seen a surge in interest because of their unique physicochemical properties, including low vapor pressure, high thermal stability, non-flammability, large electrochemical window, and tunability of physicochemical properties by modification of the chemical structure.[1–3] These properties make them attractive for a wide range of applications.[4,5] Notwithstanding their assumed huge potential, industry is still reluctant to widely apply these solvents.[6] Although theoretically an astronomical number of ionic liquids could be designed and the properties of many ionic liquids have been described in the literature, only a limited number of ionic liquids is commercially available, and an even smaller number is used on a regular basis. The ionic liquids can be classified into two broad classes: water-miscible (hydrophilic) and water-immiscible (hydrophobic) ionic liquids. One of the better known hydrophobic ionic liquids is the quaternary phosphonium ionic liquid trihexyltetradecylphosphonium chloride, $[P_{66614}]^+Cl^-$, which is produced by the company CYTEC (now part of Syensqo) and commercialized under the name Cyphos® IL 101.[7,8] Hereafter, we will abbreviate Cyphos IL 101 to C101.

Because the chemical structure of C101 is similar to that of the widely used basic extractant Aliquat 336, which is a quaternary ammonium salt with trioctylmethylammonium chloride as the main component, it is not surprising that the *solvent extraction* (SX) of metal ions by C101 has been the topic of many research studies.[9–17] Arguments that have been used to prefer C101 over Aliquat 336 are the lower solubility of C101 in the raffinate due to its longer alkyl chains and the higher selectivities and extraction efficiencies that can be obtained with C101.[9,18–21] Surprisingly high losses up to 3.7 $g \cdot L^{-1}$ in the raffinate have been reported for C101, which is in strong contrast with its expected behavior based on the compound's hydrophobicity.[21] A recent study demonstrated that the solubility of C101 in ethylene glycol

View Article Online
DOI: 10.1039/D5RE00536A

solutions was overestimated by an order of magnitude based on phosphorus ICP-OES analysis, highlighting the importance to investigate C101 solubility losses during separation processes more thoroughly.[22] This discrepancy was attributed to the presence of significant amounts of phosphor-based impurities in the C101 product, which are more soluble than the main component in C101, being $[P_{66614}]^+Cl^-$. The presence of these impurities may not only lead to erroneous conclusions about the losses of C101 during SX, but they can also alter C101's performance as extractant. The effect of impurities on the extraction behavior is particularly relevant, since the main impurities, phosphane oxides and protonated phosphanes, can act as extractants themselves. Sert *et al.* investigated the separation of thorium from cerium and lanthanum.[17] The small, but significant co-extraction of the lanthanides is noteworthy, as previous studies by Reddy *et al.*[23] and Hui *et al.*[24] had demonstrated that lanthanide ions can be extracted by phosphane oxide extractants. Since these phosphane oxides are present in C101 as well, the former study might have underestimated the selectivity of pure $[P_{66614}]^+Cl^-$. Similar issues may arise with protonated phosphanes, analogous to the commonly used protonated amines, which are known to extract a wide variety of metals.[25] Although the phosphorus-based alternatives of the trialkylamines, *i.e.* the trialkylphosphanes, are not commercially viable extractants since they are easily oxidized to the corresponding oxides, these compounds can extract metals in their protonated form as well. Furthermore, the impurities may contaminate downstream solutions, necessitating additional attention during subsequent processing steps.

It is well established that the synthesis of ionic liquids often results in the presence of impurities arising from side reactions, incomplete conversion, thermal degradation, contamination of starting materials, or residual byproducts.[26–28] Common purification strategies for ionic liquids include washing, distillation, recrystallization, treatment with activated charcoal, solvent extraction, and column chromatography.[26–32]

View Article Online
DOI: 10.1039/D5RE00536A

Among these approaches, activated charcoal treatment is one of the most straightforward and has been widely applied for the decolorization of ionic liquids.[29,33,34] However, this method is generally only suitable for already highly pure IL samples where only trace amounts of colored contaminants remain. Furthermore, activated charcoal treatment is ineffective for several classes of ionic liquids. In particular, halide-containing systems often cannot be fully decolorized using this approach.[33,35] In the case of trihexyl(tetradecyl)phosphonium diisobutylphosphate, the formation or dissolution of colored species upon charcoal treatment has even been reported.[33] Consequently, due to both the large impurity load (*vide infra*) and the apparent chemical compatibility issues with the $[P_{66614}]^+$ cation, activated charcoal purification is considered unsuitable for $[P_{66614}]^+Cl^-$ purification.

Evaporation-based purification represents another straightforward strategy and has frequently been employed for the removal of volatile impurities, or even for removal of the ionic liquids themselves.[27,28,36] This approach is particularly attractive because it can, in principle, separate ionic liquids from high-boiling residual compounds or side products.[37] Nevertheless, distillation-based purification is not appropriate for C101 because of its limited thermal stability.[38] In addition to degradation concerns, evaporation of ionic liquids itself presents major drawbacks. Such processes typically rely on Kugelrohr-type apparatuses, which are inherently limited in throughput and difficult to scale toward larger processing volumes.

Crystallization methods have likewise proven successful for several ionic liquid systems.[29,39] For example, residual lead impurities formed during the synthesis of 1-ethyl-3-methylimidazolium ethanoate were selectively removed through crystallization.[40] However, crystallization is not feasible for C101 or its associated side products, as no crystallization occurs before reaching the glass transition temperature of the ionic liquid.[41]

View Article Online
DOI: 10.1039/D5RE00536A

Another commonly employed strategy for obtaining highly pure ionic liquids involves minimizing impurity formation during synthesis itself through the use of higher-purity starting materials, optimized reaction conditions, or alternative synthetic pathways.[27,28] Such approaches can substantially reduce the purification burden and are frequently preferred over extensive downstream purification. However, for ionic liquids intended for SX of metal ions, this strategy is often economically unattractive. Extractants such as C101 already represent relatively high-value specialty chemicals, and further increasing reagent purity or employing more elaborate synthetic routes would substantially increase production costs. Therefore, efficient post-synthetic purification strategies is believed to remain of greater practical relevance for such systems.

Consequently, liquid–liquid extraction remains the only practically viable purification strategy for C101. Such approaches are widely employed in ionic liquid purification and have proven effective for the removal of inorganic salts, acids, and other polar impurities from hydrophobic ionic liquids through one or multiple water washing steps.[27,42] Continuous reflux-based purification methodologies have also been described for the removal of inorganic salts, halide residues, and alkali metal impurities from hydrophilic ionic liquids using solvents such as dichloromethane, ethyl acetate, and tetrahydrofuran.[42] Related approaches have further been proposed for halide-based ionic liquids, including an energy-efficient Soxhlet/Dean–Stark hybrid setup described by Bogdanov *et al*.[43]

Nevertheless, the removal of structural isomers and closely related side products remains significantly more challenging because of their highly similar solubility behavior, which limits selective separation. In such cases, chromatographic methods may offer advantages by enabling separation of structurally related compounds, including isomers differing in alkyl chain length or branching.[32] However, purification by chromatography remains highly restrictive for large-scale production because of its high solvent consumption, low throughput,

View Article Online
DOI: 10.1039/D5RE00536A

and limited scalability compared with separation technologies such as solvent extraction, which are inherently more suitable for implementation in the industry.

To the best of our knowledge, the application of these methods to C101 has been reported only once, in a study by Deferm *et al*. In that work, a three-step purification protocol was employed, consisting of an initial NaOH wash, followed by pH neutralization using deionized water, and finally multiple washing steps with hot heptane under reflux conditions. Although a purity of 99.5% was reported, the relatively short recycle delay time used in the NMR measurements may have compromised the quantitative accuracy. In addition, significant broadening of the phosphane oxide signal was observed in the absence of polar protic solvents such as methanol or ethylene glycol (*vide infra*), which likely resulted in an underestimation of the phosphane oxide impurity content and therefore further compromised the quantitative reliability of the analysis.

Hence, the procedure reported by Deferm *et al.* remains the only documented purification strategy for this commercially available ionic liquid, despite several notable limitations. The method is labor-intensive, inefficient, and requires numerous prolonged heptane reflux steps. Moreover, strong batch-to-batch variability has been observed.[44] This lack of reproducibility is particularly problematic and highlights the need for a more systematic investigation into the origin of these inconsistencies.

In our recent work, we demonstrated that impurities present in C101 exhibit higher solubility in ethylene glycol than the $[P_{66614}]^+Cl^-$ ionic liquid itself. This finding suggests that ethylene glycol-based purification strategies may be promising. Furthermore, our study indicated that the purity of commercially available C101 is likely overestimated compared to manufacturer specifications, emphasizing the need for improved analytical and purification methodologies.[22]

View Article Online
DOI: 10.1039/D5RE00536A

In the present study, the main and minor impurities in C101 are identified using *liquid chromatography–mass spectrometry* (LC–MS). In addition, ^{31}P NMR spectroscopy was used to identify and quantify the main impurities in the commercial product and key limitations associated with these measurements are addressed. Finally, a continuous *non-aqueous solvent extraction* (NASX) process employing ethylene glycol is proposed for the purification of C101 at liter scale.

Experimental

Chemicals

Seven different batches of trihexyltetradecylphosphonium chloride, Cyphos® IL 101 (C101), were obtained from Cytec Sàrl (Faulquemont, France) and IoLiTec GmbH (Heilbronn, Germany). The actual batch numbers can be found in Table S1 of the Supplementary Information (SI). 1000 mg·L^{-1} standard solutions of phosphorus and scandium in 2 – 5 % nitric acid were purchased from Chem-Lab (Zedelgem, Belgium). Ethylene glycol (99.5 %) was obtained from Acros Organics (Geel, Belgium). Ultrapure water (18.2 MΩ·cm) was generated using a Merck Millipore Milli-QTM Reference Ultrapure Water Purification System. Sodium chloride (99.5 %) was obtained from Thermo Fisher Scientific (Geel, Belgium). CD_3OD (99.8 atom% D), $CDCl_3$ (99.8 atom% D), and D_2O (99.8 atom% D) were obtained from Merck Life Science (Darmstadt, Germany). All products were used as received, without any further purification unless stated otherwise.

Nuclear magnetic resonance spectroscopy

View Article Online
DOI: 10.1039/D5RE00536A

^{31}P and $^{31}P\{^{1}H\}$ NMR spectra were recorded on a Bruker Avance Neo 600 spectrometer with a Bruker Ascend™ 600 magnet system fitted with a 5 mm triple-resonance PI HR-TBO (BB (^{31}P-^{75}As/^{139}La-^{109}Ag)/F-H/F-D) SmartProbe iProbe with z-gradients and ATM accessory for Automatic Tuning and Matching. Data acquisition and processing was performed using Topspin 4.5.0 software. Measurements were performed in Norell® Standard Series™ 5 mm NMR tubes, containing a custom reference tube, with an outer diameter of 1.62 ± 0.02 mm and an inner diameter of 1.20 ± 0.02 mm, inserted in the center. A 5 wt% H_3PO_4 solution containing D_2O was used as external reference unless stated differently. 200 µL of the C101 phase, after contact with the ethylene glycol phase, was diluted in 250 µL of methanol unless stated otherwise. Delay times were 8 seconds for measurement of ^{31}P in MeOH, 10 seconds for $^{31}P\{^{1}H\}$ in MeOH, and 100 seconds for $^{31}P\{^{1}H\}$ in $CDCl_3$.

Liquid chromatography-mass spectrometry (LC-MS)

The minor impurities in C101 were characterized by LC-MS analysis using a Shimadzu LCMS-2020 mass spectrometer in positive-ion mode coupled to a Shimadzu Prominence-i-LC-2030C 3D plus autosampler and pump. Electrospray ionization (ESI) was employed for all measurements. Separation was achieved on an InfinityLab Poroshell 120 EC-C18 column (2.1 × 100 mm, 2.7 µm particle size, 120 Å pore size).

All, but one, samples were prepared by dissolving C101 in neat methanol with a final concentration of 1 $g \cdot L^{-1}$. Separation over the column was achieved by a gradient approach with two mobile phases. Mobile phase A consisted of water with 0.1 $mol \cdot L^{-1}$ formic acid, and mobile phase B consisted of methanol with 0.1 $mol \cdot L^{-1}$ formic acid. The gradient began at 50% A + 50% B, ramped linearly to 100% B over 30 min, then was held at 100% B for an additional 15 min (SI, Figure S1). The flow rate was set to 0.350 $mL \cdot min^{-1}$, and the injection

View Article Online
DOI: 10.1039/D5RE00536A

volume was 1 µL. One sample was prepared in neat acetonitrile instead and analyzed under identical LC-MS conditions, with methanol containing 0.1 mol·L^{-1} formic acid substituted by acetonitrile containing 0.1 mol·L^{-1} formic acid in the mobile phase as well.

Batch purification process

Multistep batch-scale purifications were performed by contacting a presaturated C101 phase with fresh ethylene glycol solution containing 0.2 mol·L^{-1} NaCl. All samples were mixed for 1 hour using a RS-1 separatory funnel shaker at 300 rpm and 21 ± 0.5 °C. The solution was left to naturally disengage before removal of the ethylene glycol phase after contact and subsequent addition of neat ethylene glycol solution for the following extraction step. Samples of the C101 phase were taken for LC-MS and ^{31}P NMR at each stage and centrifuged at 3000 rpm for 5 min in an Eppendorf centrifuge 5804 to accelerate phase disengagement.

Extraction kinetics of the process were determined by contacting 9 identical samples of C101 with ethylene glycol containing 0.2 mol·L^{-1} NaCl. Samples were rapidly disengaged using the Eppendorf centrifuge 5804 centrifuge at 5000 rpm at multiple time intervals (10, 20, 30, 60, 120, 240, 300, 600, and 1200 seconds). The phosphorus content in the ethylene glycol solution after contact was subsequently determined using *inductively coupled plasma–optical emission spectroscopy* (ICP-OES). ICP-OES analysis was performed using a PerkinElmer Avio 500 equipped with a GemCone high solids nebulizer, baffled cyclonic spray chamber, 2.0 mm inner diameter alumina injector, and a PerkinElmer Hybrid XLT torch. The plasma, auxiliary, and nebulizer gas flows were set to 10 L·min^{-1}, 0.2 L·min^{-1}, and 0.7 L·min^{-1}, respectively. Samples were prepared by diluting 100 µL of the ethylene glycol solution (after contact with C101) and 50 µL of a 1000 mg·L^{-1} scandium standard solution to a final volume of 10 mL, using a 2 vol% HNO_3 solution in ultrapure water. A calibration curve was

View Article Online
DOI: 10.1039/D5RE00536A

constructed with a series of calibration samples containing 0, 1, 2, 4, 8, 12, 16, and 20 mg·L^{-1} phosphorus. The calibration samples were prepared by diluting 50 µL of a 1000 mg·L^{-1} scandium standard solution, 100 µL of ethylene glycol solution (before contact with C101), and the appropriate amount of a 1000 mg·L^{-1} phosphorus standard solution to a final volume of 10 mL, using a 2 vol% HNO_3 solution in ultrapure water. The addition of 100 µL of ethylene glycol solution ensured matrix matching. Scandium served as an internal standard throughout. Spectral lines 357.253 nm and 178.221 nm were used for scandium and phosphorus, respectively. All measurements were carried out in axial view mode.

Physical properties of solvent extraction streams

The viscosity and density of both streams were measured using an Anton Paar Lovis 2000 ME rolling-ball viscometer coupled with a DMA 4500 M oscillating U-tube density module. Settling velocities of the C101 phase in ethylene glycol solutions containing 0.2, 0.4, 0.6, and 0.8 mol·L^{-1} NaCl were determined at 21, 40, and 60 °C in a 250 mL glass beaker (12.3 × 7.0 × 6.8 cm) at a 1:1 phase ratio, using 50 mL of each phase. Mixing was performed with a rotating disk impeller for 10 min, after which the impeller was stopped and the time to complete phase disengagement was recorded. The distance to the interphase was measured with a caliper. All experiments were conducted under ethylene glycol phase continuity, ensured by positioning the impeller in the center of the ethylene glycol phase. The temperature was controlled using a IKA RCT basic magnetic stirrer and heating plate connected to a IKA ETS-D5 contact thermometer. A schematic of the experimental setup is shown in Figure S2 (SI).

Continuous purification process using an agitated counter-current column

View Article Online
DOI: 10.1039/D5RE00536A

Continuous counter-current purification of C101 was performed employing a Kühni ECR32 agitated laboratory column (Sulzer, Switzerland), comprised of 5 sections, with a total column volume of 3 L. A schematic representation of the setup is shown in Figure 1. Agitation was achieved with a PEEK rotor-stator assembly driven by a turbine agitator mounted atop the column (SI, Figure S3).

The column was maintained at 60 °C using a Haake DC10 recirculating water bath that pumped water at 60 °C through the glass outer jacket. To mitigate major temperature gradients throughout the column, the solutions were preheated to 60 °C via a custom heater comprised of a glass cylinder wrapped with a RS Pro heating mat controlled by a Delta Electronics DTK PID Temperature Controller connected to a RS PRO PT1000 RTD sensor. Two Cole-Parmer Masterflex L/S Precision Variable-Speed Console Drives, each fitted with an Easy-Load pump head, delivered the ethylene glycol and C101 phases through Masterflex Tygon Chemical L/S Precision Pump Tubing, which was used throughout the entire column.

View Article Online
DOI: 10.1039/D5RE00536A

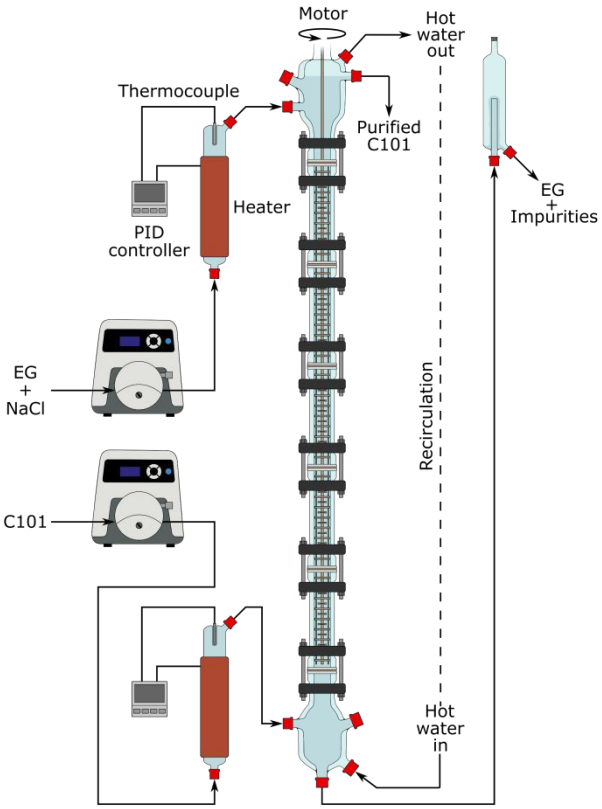

Figure 1. Schematic representation of the Kühni agitated column setup.

Results and discussion

Synthetic background of Cyphos IL 101

To determine the impurities present in C101, it is necessary to first shortly consider the synthesis route used for its production, as this defines the range of species that may be present in the commercial product. C101 is synthesized via a two-step process. In the first step, trihexylphosphane is produced by radical addition of 1-hexene to phosphane (Figure 2.a).[38] In the second step, the resulting trihexylphosphane is alkylated with 1-chlorotetradecane at elevated temperature, forming the corresponding quaternary phosphonium salt, $[P_{66614}]^+Cl^-$ (Figure 2.b).[7]

View Article Online
DOI: 10.1039/D5RE00536A

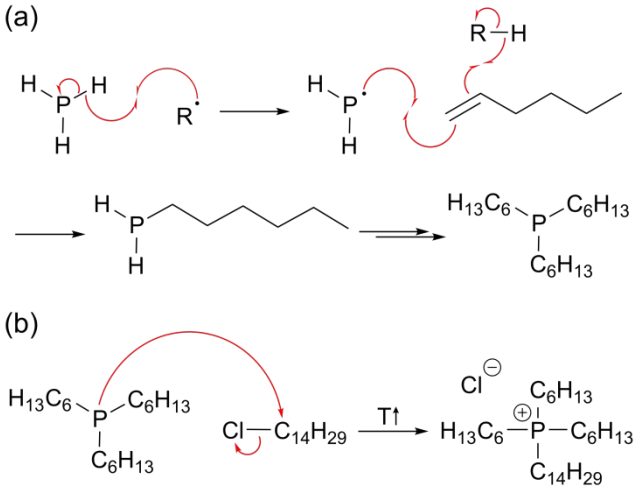

Figure 2. Two-step synthesis route of C101 showing (a) the formation of trihexylphosphane and (b) the subsequent alkylation reaction with 1-chlorotetradecane at elevated temperature.

LC-MS analysis

Mass spectrometry, coupled with liquid chromatography, (LC-MS) was employed to investigate the chemical composition of C101 (Table 1). Liquid chromatography not only simplifies analysis of the mass spectra by separating the species prior to analysis, but also allows verification of the existence of isomers, and the technique is able to differentiate between products found in the original solution and the ones formed during ionization.

Before delving into the mass spectral analysis, it is important to note that no distinction can be made between trihexylphosphane and its protonated form, the trihexylphosphonium cation. To avoid confusion, the notation of $[M]^+$ is used to refer to the phosphonium cations, as they are the dominant species in solution, as illustrated by NMR analysis (*vide infra*). Moreover, it is important to note that unambiguous assignment of several species is not feasible, as different chain length combinations can result in identical *m/z* values.

View Article Online
DOI: 10.1039/D5RE00536A

LC-MS analysis of the commercial samples revealed numerous signals. A particularly intense signal of *m/z* = 317.3 coeluted with the $[M]^+$ signal of trihexylphosphonium chloride (*m/z* = 287.3), corresponding to the unreacted starting material from the alkylation step, at retention times of 12.4 and 13.6 minutes (Figure 3). To the best of our knowledge, this signal cannot be attributed to any known or expected impurity based on the published synthesis route.[7] Furthermore, the signal at *m/z* = 287.3 is unexpectedly weak despite the inherent positive charge of the phosphonium cation. A comparison of the signal intensity with that of a structurally related, but less abundant homologue (*e.g.*, dihexyltetradecylphosphonium chloride) further corroborates the unusually low intensity for *m/z* = 287.3 (SI, Figure S4).

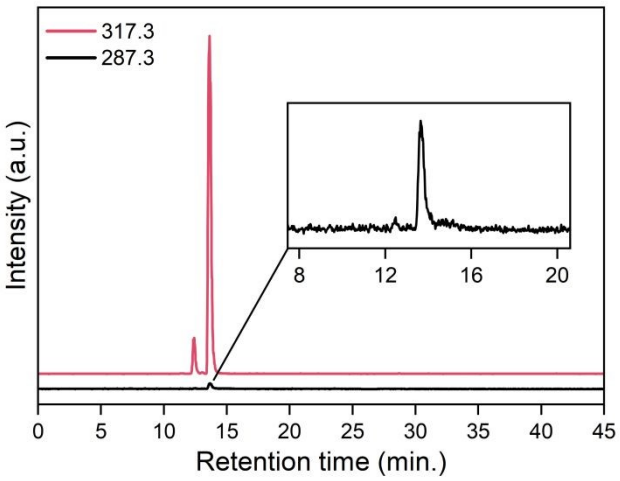

Figure 3. Extracted ion chromatogram of m/z = 287.3 and 317.3 (LC-MS, Batch 2).

The signal of *m/z* = 317.3 was found to be only consistent with the trihexyl(methoxy)phosphonium cation, most likely generated via a gas-phase reaction between trihexylphosphane and methanol occurring during electrospray ionization. This hypothesis accounts for the identical retention times of both species despite their structural differences, as well as the unexpectedly low intensity of the *m/z* = 287.3 signal. To test this

View Article Online
DOI: 10.1039/D5RE00536A

hypothesis, the LC-MS analysis was repeated using acetonitrile in place of methanol. Under these conditions, an intense *m/z* = 287.3 signal at 5.35 minutes appeared, whereas the major coeluted signal (*m/z* = 317.3) observed in methanolic solutions was absent, supporting the occurrence of a methanol-induced gas-phase reaction (SI, Figure S5-6).

In addition to these observations, the occurrence of two distinct maxima at different elution times strongly indicates the presence of structural isomers. In fact, less abundant species, eluting slightly earlier, is consistently observed across multiple chromatograms with a relative intensity of approximately 8%. All these minor components can be attributed to the hexan-2-yl variants of the corresponding linear species. Their presence can be rationalized based on the industrial synthesis route of $[P_{66614}]^+Cl^-$. Although radical additions favor anti-Markovnikov selectivity, a small but notable fraction occurs via Markovnikov addition at the more substituted carbon of 1-hexene (Figure 4). This less-favored isomer is thus inadvertently incorporated into the subsequent alkylation step with 1-chlorotetradecane. Hence, a wide variety of hexan-2-yl analogues can be observed in the commercial product.

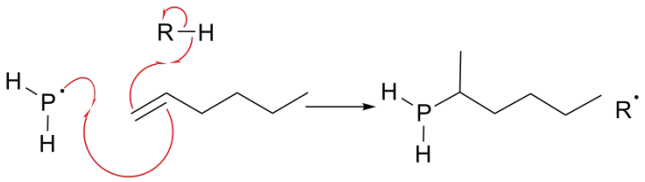

Figure 4. Markovnikov addition of 1-hexene to phosphane.

Two additional $[M]^+$ signals corresponding to dodecyldihexylphosphonium chloride (*m/z* = 371.3) and dihexyltetradecylphosphonium chloride (*m/z* = 399.5), were detected, exhibiting notably longer retention times of 18.3 and 20.9 minutes, respectively (SI, Figure S7). Although these species were previously believed to arise from onium fragmentation of the

View Article Online
DOI: 10.1039/D5RE00536A

$[P_{66614}]^+Cl^-$ compound during ionization[38], their distinct retention times refute this hypothesis and suggest the presence of these compounds prior to ionization. Both species are most likely formed through the reaction of residual dihexylphosphane, an intermediate generated during the synthesis of trihexylphosphane, with 1-chlorotetradecane and its shorter homologue, 1-chlorododecane, present in smaller amounts (Figure 5.a). Additionally, a reversed Menshutkin-type reaction involving the hexyl substituents during the final synthesis step of $[P_{66614}]^+Cl^-$ might also contribute to their presence (Figure 5.b).

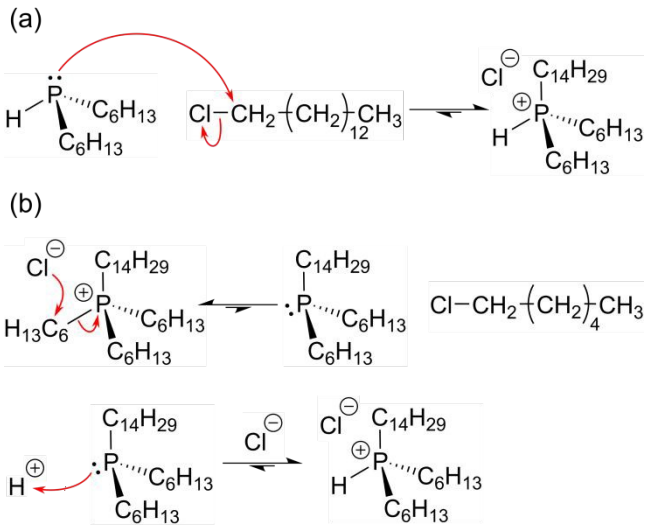

Figure 5. Proposed reaction pathways for the formation of dihexyltetradecylphosphonium chloride by (a) the reaction of residual dihexylphosphane and (b) a reversed Menshutkin-type reaction.

Alongside the phosphonium species, their corresponding phosphane oxides were also detected. Owing to their non-ionic nature, these compounds exhibit a broad range of adducts, including $[M + H]^+$, $[M + MeOH + H]^+$, $[M + MeOH + Na]^+$, $[2M + H]^+$, and $[2M + Na]^+$ (SI, Figure S8). One phosphane oxide, dihexylphosphane oxide, for which no protonated

View Article Online
DOI: 10.1039/D5RE00536A

phosphane counterpart was detected, has been identified as well (SI, Figure S9-12). Its absence is expected, as residual dihexylphosphane readily reacts with oxygen.[45] Furthermore, hexyldihexylphosphinate was identified (*m/z* = 319.3; SI, Figure S10-12). Phosphinate species are known to form alongside phosphane oxides during the autoxidation of phosphanes.[46]

A remarkable variety of $[P_{66614}]^+Cl^-$ analogues were also detected by LC-MS. Most of these analogues can be attributed to impurities in the 1-hexene and 1-chlorotetradecane reagents used for C101 production, which differ in alkyl chain length. The presence of the dodecyldihexyltetradecylphosphonium (*m/z* = 567.7) and dihexylditetradecylphosphonium (*m/z* = 595.7) cations indicate the subsequent reaction of dodecyldihexylphosphonium chloride and dihexyltetradecylphosphonium chloride with an additional 1-chlorotetradecane molecule (SI, Figure S13).

The detection of three ions at *m/z* = 425.5, 453.5, and 481.5 (SI, figure S14), each 2 Da lower than the main $[P_{66614}]^+Cl^-$ signal (*m/z* = 483.6) and its shorter analogues (m/z 427.4 and 455.5), indicates the introduction of a single C=C double bond into the alkyl chains. Their distinct retention times rule out in-source fragmentation, pointing instead to the reaction of phosphane with trace amounts of hexadiene (*e.g.*, 1,5-hexadiene) or alkyne (*e.g.*, 1-hexyne) impurities commonly found in commercial 1-hexene[47,48], subsequently leading to the formation of the observed unsaturated phosphonium species.

View Article Online
DOI: 10.1039/D5RE00536A

Table 1. Summary of LC-MS data.†

Retention time (min)	m/z (± 0.1)	Observed ion	Compound
			hexan-2-yldihexylphosphonium chloride
12.4	287.3	$[M]^+$	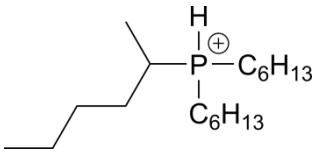
			hexan-2-yldihexylmethoxyphosphonium chloride
12.4	317.3	$[M]^+$	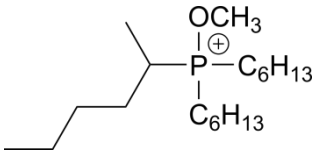
			trihexylphosphonium chloride
13.6	287.3	$[M]^+$	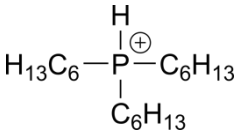
			trihexylmethoxyphosphonium chloride
13.6	317.3	$[M]^+$	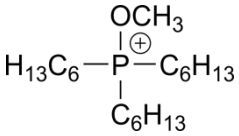
			hexan-2-ylhexylphosphane oxide
	219.2	$[M + H]^+$	
14.2	251.2	$[M + CH_3OH + H]^+$	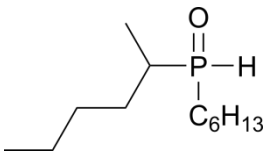
	273.2	$[M + CH_3OH + Na]^+$	
	219.2	$[M + H]^+$	
	251.2	$[M + CH_3OH + H]^+$	dihexylphosphane oxide
15.2	273.2	$[M + CH_3OH + Na]^+$	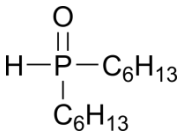
	437.3	$[2M + H]^+$	
	459.3	$[2M + Na]^+$	
			dodecyldihexylphosphonium chloride
18.3	371.3	$[M]^+$	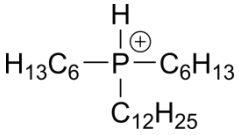
			dihexyltetradecylphosphonium chloride
20.9	399.5	$[M]^+$	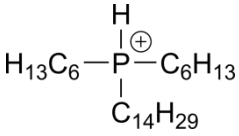
22.1 & 22.7	425.5	$[M]^+$	decylhexenyldihexylphosphonium chloride/ butyldodecylhexenylhexylphosphonium chloride/

			dibutylhexenyltetradecylphosphonium chloride§
23.1 & 25.1	427.4	$[M]^+$	decyltrihexylphosphonium chloride/ butyldodecyldihexylphosphonium chloride/ dibutylhexyltetradecylphosphonium chloride 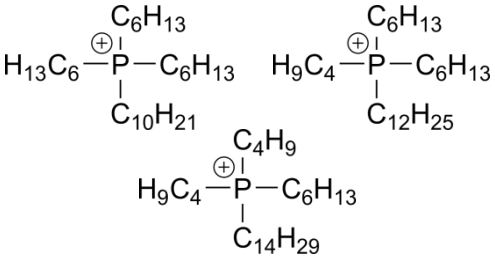
24.0	303.2	$[M + H]^+$	hexan-2-yldihexylphosphane oxide 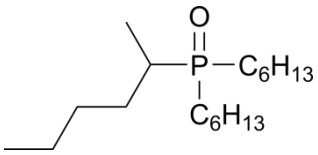
	335.3	$[M + CH_3OH + H]^+$	
	357.3	$[M + CH_3OH + Na]^+$	
	605.6	$[2M + H]^+$	
	627.6	$[2M + Na]^+$	
24.2 & 24.8	453.5	$[M]^+$	dodecylhexenyldihexylphosphonium chloride/ butylhexenylhexyltetradecylphosphonium chloride§
24.3	303.2	$[M + H]^+$	trihexylphosphane oxide 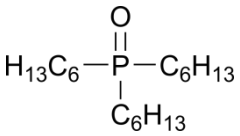
	335.3	$[M + CH_3OH + H]^+$	
	357.3	$[M + CH_3OH + Na]^+$	
	605.6	$[2M + H]^+$	
	627.6	$[2M + Na]^+$	
25.0 & 25.6	455.5	$[M]^+$	dodecyltrihexylphosphonium chloride/ butyldihexyltetradecylphosphonium chloride 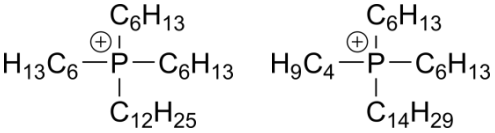
25.1	481.6	$[M]^+$	hexan-2-ylhexenylhexyltetradecylphosphonium chloride§
25.6	483.6	$[M]^+$	trihexyltetradecylphosphonium chloride/hexan-2-yldihexyltetradecylphosphonium chloride
	1002	$[2M + Cl]^+$	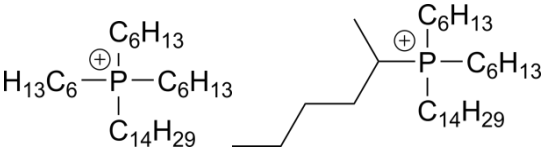
	1012	$[2M + HCOO]^+$	
25.7	481.6	$[M]^+$	hexenyldihexyltetradecylphosphonium chloride§
27.2	319.3	$[M + H]^+$	hexyldihexylphosphinate 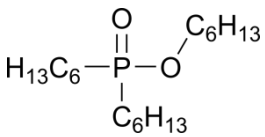
27.3, 27.7, 28.0 & 28.4‡	511.6	$[M]^+$	hexan-2-ylhexyloctyltetradecylphosphonium chloride/hexadecylhexan-2-yldihexylphosphonium

View Article Online
DOI: 10.1039/D5RE00536A

			chloride/dihexyloctyltetradecylphosphonium chloride/hexadecyltrihexylphosphonium chloride 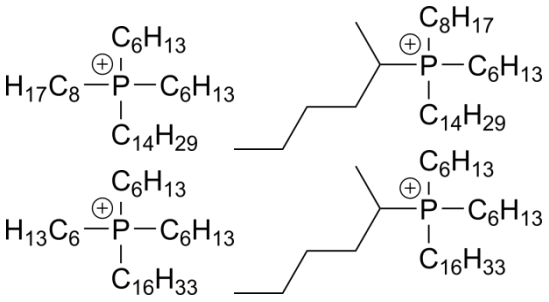
29.4	567.7	$[M]^+$	dodecyldihexyltetradecylphosphonium chloride/ butylhexylditetradecylphosphonium chloride 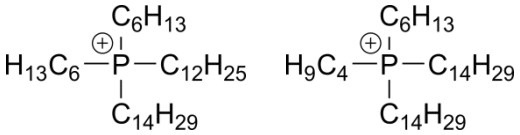
30.5	387.4	$[M + H]^+$	dodecyldihexylphosphane oxide/ butylhexyltetradecylphosphane oxide 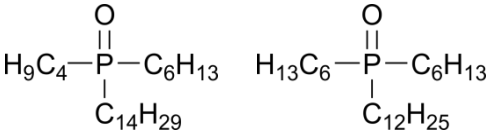
30.8	595.7	$[M]^+$	dihexylditetradecylphosphonium chloride 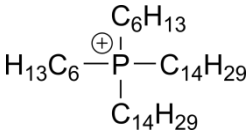
	415.4	$[M + H]^+$	dihexyltetradecylphosphane oxide
32.6	437.4	$[M + Na]^+$	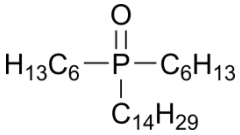

† LC–MS data from multiple batches were analyzed. Identical signals were observed throughout. However, small inter-batch shifts in retention time were noted, and the retention times reported here correspond to Batch 2.

□ The retention time of the main $[P_{66614}]^+Cl^-$ species appears as an interval (25.6–27.4 min.) as a result of its high concentration. A retention time of 25.6 minutes was obtained after an additional 100-times dilution.

‡ SI, Figure S15

§ The double bond can occupy several different positions along the alkyl chain, giving rise to multiple structural isomers (SI, Figure S16).

^{31}P NMR analysis of C101 in deuterated chloroform

Although phosphorus-31 NMR (^{31}P NMR) spectroscopy is primarily conducted using methanolic solutions in this study, a brief introduction to the use of $CDCl_3$, commonly employed for C101 analysis, and its corresponding pitfalls is warranted. Figure 6 illustrates the proton-decoupled spectrum ($^{31}P\{^1H\}$) of pure C101 diluted in $CDCl_3$. The overall chemical shift values are consistent with literature data.[15,49] The main $[P_{66614}]^+Cl^-$ compound, observed at δ = 33.48 ppm, is accompanied by two sets of satellite peaks, both arising from coupling with carbon-13 ($^1J_{PC}$ = 47.1 Hz and $^{2/3}J_{PC}$ = 14.5 Hz). The exact origin of the latter coupling constant remains unclear, as the distinction between $^2J_{PC}$ and $^3J_{PC}$ for phosphonium type compounds is often unpredictable and can closely match each other in value.[50]

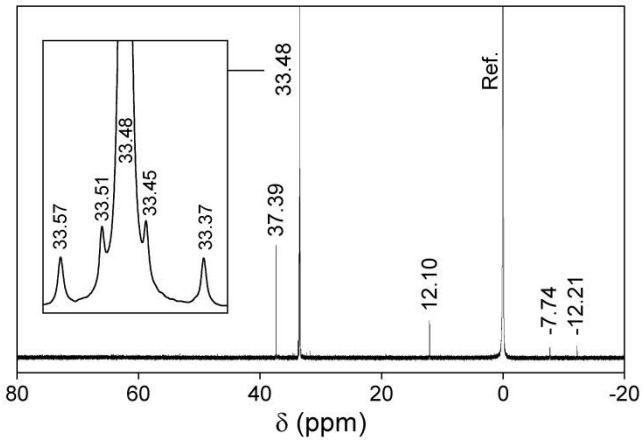

Figure 6. $^{31}P\{^1H\}$ NMR spectrum of C101 dissolved in $CDCl_3$. Conditions: 200µL of C101 (Batch 1), 250 µL of $CDCl_3$; Internal reference: 85 wt% $H_3PO_{4,aq}$.

Remarkably, the NMR spectrum does not contain any signal beyond δ = 38 ppm. This is unexpected, as C101 is known to contain phosphane oxides, as corroborated by LC-MS analysis (*vide supra*), which resonate at this higher chemical shift range. Measurement of the same sample with the addition of 30 µL of ethylene glycol does reveal a resonance in this

View Article Online
DOI: 10.1039/D5RE00536A

region, confirming the presence of trihexylphosphane oxide (Figure 7). A comparable suppression followed by the sudden appearance of a phosphane oxide resonance can be observed in a study by Onghena *et al.* as well, yet this phenomenon was neither explained nor explicitly mentioned.[49] In their study, no phosphane oxide signals are visible in neat C101, but emerge after a single contact with an aqueous solution.

Major exponential line broadening of the NMR spectrum from the sample of C101 dissolved in neat $CDCl_3$ reveals the presence of a highly broadened signal in the sample at the phosphane oxide region (Figure 7). The origin of this behavior can thus be related with major exchange broadening which occurs when the exchange rate between the two compositions is comparable to the frequency separation between their corresponding peaks.[51]

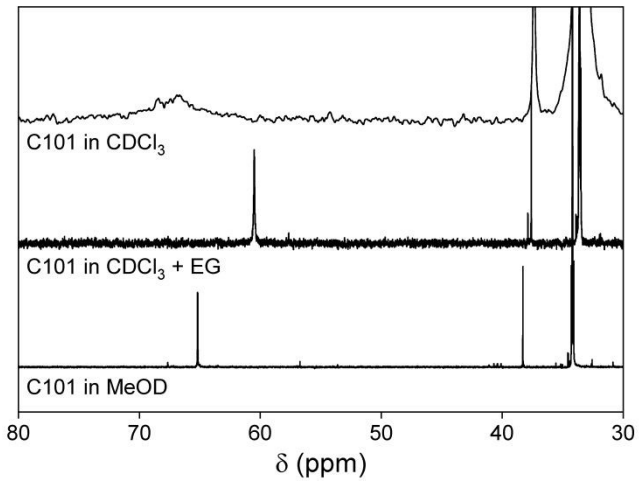

Figure 7. $^{31}P\{^{1}H\}$ NMR spectra of neat C101 in different solvents: (a) $CDCl_3$ (200 µL of C101 (Batch 1), 250 µL $CDCl_3$, LB = 40), (b) MeOD (200 µL of C101 (Batch 1), 250 µL of MeOD, LB = 1), (c) $CDCl_3$ + ethylene glycol (170 µL of C101 (Batch 1), 30 µL of ethylene glycol, 250 µL of $CDCl_3$); Internal reference: 85 wt% $H_3PO_{4,aq}$.

View Article Online
DOI: 10.1039/D5RE00536A

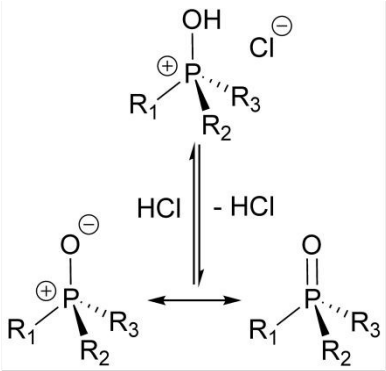

Figure 8. Acid/base equilibrium for phosphane oxides.

The presence of two chemical forms for the phosphane oxide species can only be attributed to an acid/base equilibrium (Figure 8) in which the oxygen atom is protonated. Therefore, introducing protic solvents such as ethylene glycol or methanol accelerates the proton exchange process, pushing the system into the fast-exchange regime and resulting in narrower NMR signals. To further support this hypothesis, the chemical shift of the phosphane oxides before and after a single contact with a concentrated HCl solution were measured (Figure 9). A major downfield shift was observed. This observation is in line with the expected reduction in double bond character of the phosphorus–oxygen bond and increase in formal positive charge on the phosphorus atom. While applying substantial line broadening may reveal the presence of a phosphane oxide signal in $CDCl_3$ solution, this approach can significantly distort conclusions if not carefully accounted for, while the low S/N ratio prevents reliable quantification.

View Article Online
DOI: 10.1039/D5RE00536A

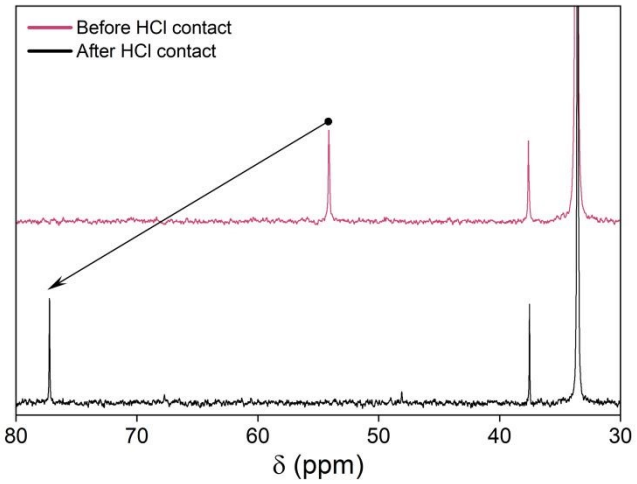

Figure 9. $^{31}P\{^{1}H\}$ NMR spectra of C101 saturated with ethylene glycol dissolved in $CDCl_3$ before and after contact with a 37% $HCl_{aq.}$ solution (200 µL of $C101_{sat.}$ (Batch 1), 250 µL of $CDCl_3$, LB = 2); Internal reference: 85 wt% $H_3PO_{4,aq}$.

^{31}P NMR analysis of C101 in methanol

As a result of the observations made in chloroform, all subsequent measurements were performed in methanol, which does not suffer from exchange broadening. Methanol also offers the added benefit of substantially shorter T_1 relaxation times (SI, Figure S17-21) allowing a reduction in delay time from 100 seconds for $CDCl_3$ to 8 seconds for methanolic solutions.[22] Unfortunately, deuterated methanol often results in less reliable locking. As a result, an external reference containing a 5 vol% H_3PO_4 solution dissolved in D_2O was used for locking and referencing instead. Comparison of the C101 NMR spectra recorded in methanol (Figure 10) and $CDCl_3$ reveals that the chemical shifts remain largely unchanged, exhibiting only minor variation as a result of differences in solvation and change in reference composition.

The main $[P_{66614}]^+Cl^-$ compound is slightly shifted downfield to δ = 33.59 ppm. A well-known and relatively large signal, more deshielded than the main $[P_{66614}]^+Cl^-$ compound, is observed

View Article Online
DOI: 10.1039/D5RE00536A

at δ = 37.66 ppm (satellite: $^{1}J_{PC}$ = 45.5 Hz), corresponding to hexan-2-yldihexyl(tetradecyl)phosphonium chloride.

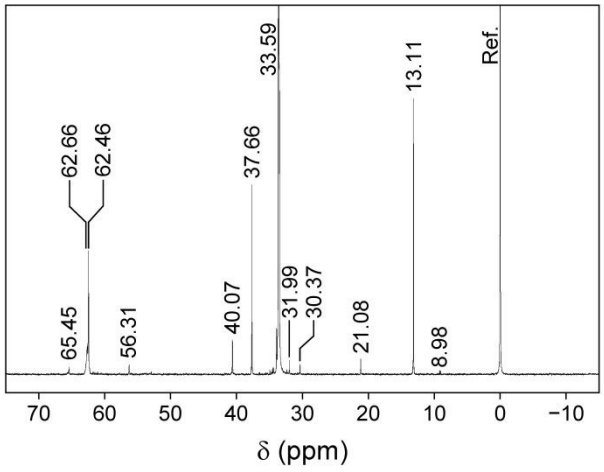

Figure 10. $^{31}P\{^{1}H\}$ NMR spectrum of neat C101 in methanol. Conditions: 200 µL of C101 (Batch 2), 250 µL of MeOH, internal reference: 5 wt% H_3PO_4 in D_2O.

Four signals characteristic of the P=O functional group were observed at δ = 56.31, 62.46, 62.66 and 65.45 ppm. The dominant signal at δ = 62.46 ppm is assigned to trihexylphosphane oxide, a common impurity which forms via autoxidation of residual trihexylphosphane. The signal at δ = 62.66 ppm, located near the main signal, most likely corresponds to structurally related phosphane oxides bearing similar alkyl substituents, differing in chain length or substitution. The signal at δ = 65.45 ppm is assigned to hexan-2-yldihexylphosphane oxide, formed by oxidation of hexan-2-yldihexylphosphane, generated during the synthesis of C101 (*vide supra*). The pronounced deshielding relative to trihexylphosphane oxide is consistent with the major effect of branching at the α-position on the alkyl substituent.[50] The remaining signal at δ = 56.31 ppm, which is substantially more shielded than the other phosphane

View Article Online
DOI: 10.1039/D5RE00536A

oxides, is most likely attributable to hexyldihexylphosphinate, as phosphinates are known to resonate upfield in comparison with their trialkylphosphane oxide counterparts.[50]

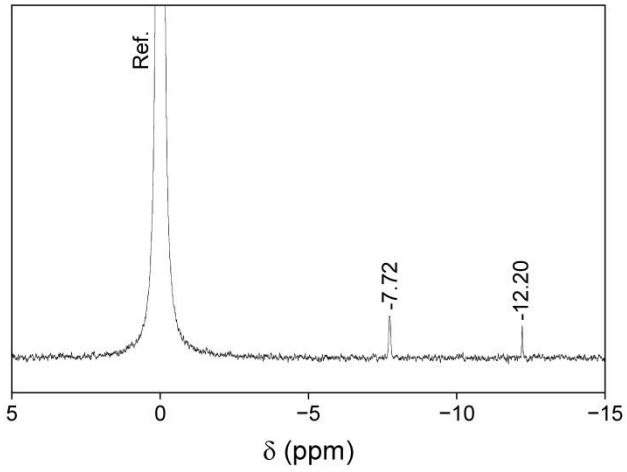

Figure 11. $^{31}P\{^{1}H\}$ NMR spectrum of neat C101 in methanol. Conditions: sample preparation was performed under argon atmosphere; 200 µL of C101 (Batch 1), 250 µL of MeOH, internal reference: 5 wt% H_3PO_4 in D_2O.

The two most shielded signals are observed at δ = –7.72 and –12.20 ppm (Figure 11), a spectral region characteristic of trialkylphosphanes. These signals were not consistently detected, neither across different samples nor within replicate measurements, suggesting a strong dependence on sample preparation. Taking special care to prevent autoxidation using argon prevented the loss of the signal, further confirming the assignment of both signals. Nevertheless, the observed signals are weak indicating an almost negligible amount of non-protonated phosphanes.

View Article Online
DOI: 10.1039/D5RE00536A

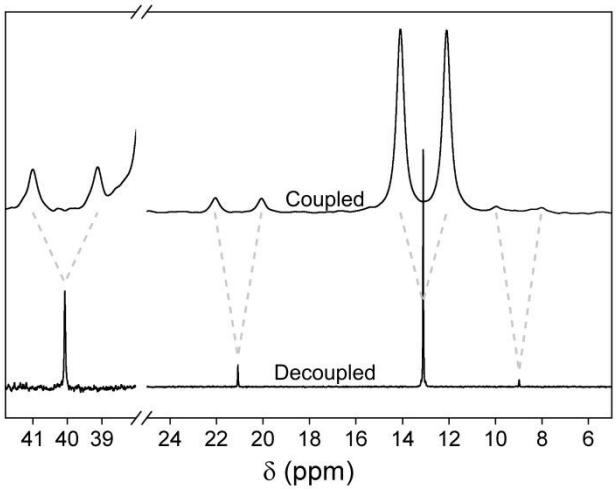

Figure 12. ^{31}P and $^{31}P\{^{1}H\}$ NMR spectra of neat C101 in methanol. Conditions: 200 µL of C101 (Batch 2), 250 µL of MeOH; internal reference: 5 wt% H_3PO_4 in D_2O; $LB_{coupled}$ = 50; $LB_{decoupled}$ = 3.

The acquisition of a proton-coupled ^{31}P NMR spectrum facilitates the assignment of signals observed at δ = 8.98, 13.11, 21.08, and 40.07 ppm (Figure 12). Each of these resonances appears as a doublet, consistent with a single one-bond phosphorus–hydrogen coupling constant ($^{1}J_{PH}$ = 474.03, 487.08, 481.61, and 463.45 Hz, respectively). This assignment is further corroborated by measurements in methanol-d_4, where characteristic deuterium-induced triplets are observed alongside a singlet (Figure 13). The singlets arise from the non-deuterated analogue of the same species, appearing slightly more deshielded than the triplets as a result of vibrational shielding for heavier isotopes.[52] This pattern confirms the presence of a direct P–H bond and supports the occurrence of proton exchange. The pronounced downfield shift of the signal at δ = 40.07 ppm is indicative of dihexylphosphane oxide, a compound also detected by LC-MS (*vide supra*). Although the signal at δ = 21.08 ppm was previously assigned to a phosphonate species[38], the presence of a doublet with a coupling constant of 481.61 Hz in the proton-coupled spectrum is incompatible with this original

View Article Online
DOI: 10.1039/D5RE00536A

assignment as no direct P–H bond can exist in that case. With the exception of dialkylphosphane oxides, only protonated phosphanes (trialkylphosphonium species) can account for proton exchange and its corresponding 1:1 splitting pattern. The presence of several protonated phosphanes at δ = 8.98, 13.11, 21.08 ppm is further corroborated by LC-MS analysis (*vide supra*), while their downfield shifts relative to the corresponding non-protonated phosphanes is well-established.[53,54]

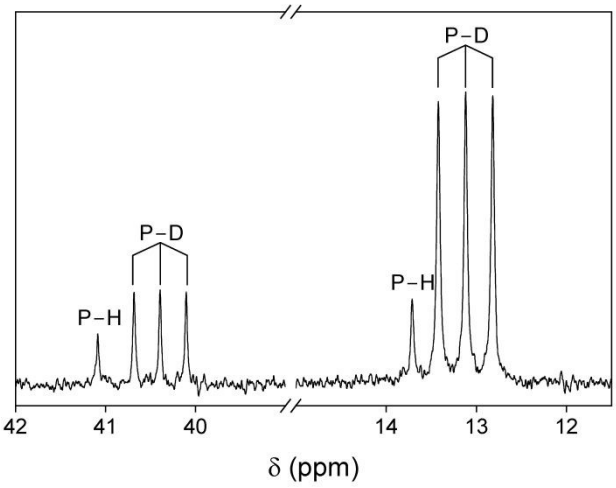

Figure 13. $^{31}P\{^{1}H\}$ NMR spectrum of neat C101 in methanol-d_4. Conditions: 200 µL of C101 (Batch 2), 250 µL of CD_3OD; internal reference: 85 wt% $H_3PO_{4,aq.}$; LB = 3.

Among these, the most intense signal at δ = 13.11 ppm can be assigned to trihexylphosphonium chloride due to its higher abundance relative to the other phosphonium species. The signal at δ = 21.08 ppm is assigned to hexan-2-yldihexylphosphonium chloride, as the additional carbon in the α-position exerts a strong electron-withdrawing effect on the phosphorus core, resulting in downfield shifting. The assignment of the remaining signal at δ = 8.98 ppm could not be established based on the ^{31}P NMR data alone.

View Article Online
DOI: 10.1039/D5RE00536A

Two additional phosphonium species, dodecyldihexylphosphonium chloride and tetradecyldihexylphosphium chloride, were identified via mass spectrometry (*vide supra*). Given the absence of other species capable of inducing $^{1}J_{PH}$ coupling, the minor signal at δ = 8.98 ppm is assigned with both species. The effect of increasing the alkyl chain length on the phosphorus nucleus diminishes rapidly for alkyl chains longer than butyl, rendering differentiation of the proposed species extremely difficult. The substantial upfield shift compared to the main trihexylphosphonium signal is, however, unexpected. Deviations in ^{31}P NMR shifting patterns are rather common for phosphorus compounds bearing bulkier substituents, as ^{31}P NMR is highly sensitive to changes in bond angles induced by steric effects.[50,55] Although the substituents of the assigned species are particularly long, they are not considered bulky, and thus the effect on bond angles is unlikely the main cause of the upfield shift. Therefore, it is hypothesized that this deviation is due to a difference in solvation, as the presence of a long linear alkyl chain can introduce surfactant characteristics, promoting aggregation with other species containing a polar functional group and long apolar alkyl chains.

Batch-to-batch variations in chemical composition

C101 has been marketed under varying purity specifications over time. Initially, suppliers reported a purity of 97.7%, whereas more recent product sheets cite minimum purities of ≥95% and, in some cases, as low as ≥93%. This downward trend could signify substantial batch-to-batch variations in chemical composition inherent to the manufacturing process. However, it most likely stems from alterations in the purity assessment protocol. In the initial report by Bradaric *et al.*, C101 was characterized as 93.9% trihexyltetradecylphopshonium chloride, 4.4% trihexylphosphonium chloride, 0.3% hydrochloric acid, and <1% of other minor impurities (e.g. dialkylphosphanes, tetradecane isomers)[7]. The original assignment of

View Article Online
DOI: 10.1039/D5RE00536A

≥97.7% purity can thus be explained by including the protonated phosphanes despite it not belonging to the tetraalkylphosphonium chloride species. Simultaneously, these result could explain the origin of the lesser cited ≥93% purity based on the trihexyltetradecylphosphonium species alone. Nevertheless, the changes in cited purity over time and the observation of major differences in the ability to purify different C101 batches indicate an additional factor at play. Therefore, batch-to-batch variations in chemical composition were investigated with seven different C101 batches.

Table 2. Batch-to-batch variations in the chemical composition of C101 based on ^{31}P qNMR.

Species Batch number†:	1	2	3	4	5	6	7
Trialkylphosphonium chlorides (%)	0	3.3	0	0	2.8	0.2	2.2
$P_{66614}Cl$ and isomers (%)	91.3	93.2	91.2	90.8	93	95.4	91.3
Hexan-2-yldihexyl (%) tetradecylphosphonium chloride (%)	1.7	2.4	1.8	1.9	2.3	1.5	1.7
Hexyldihexylphosphinate (%)	0.3	0.2	0.4	0.4	0.3	0.1	0.2
Phosphane oxides (%)	6.7	0.9	6.6	6.9	1.6	2.8	4.6

†The actual batch numbers can be found in Table S1 (SI).

Substantial differences between batches are illustrated by the qNMR results in Table 2. While the overall composition of hexan-2-yldihexyltetradecylphosphonium chloride appears relatively consistent, major variations are observed for the protonated phosphanes and phosphane oxides. Notably, the batches containing high amounts of phosphane oxides have low quantities of protonated phosphanes and *vice versa*. This observation is in line with the occurrence of an autoxidation of the protonated phosphanes over time. As direct injection of air through a sparger was found to oxidize the phosphanes within 20 seconds (*vide infra*), the existence of the trialkyl phosphonium chlorides are most likely a result of its kinetic stabilization. This hypothesis is further supported by the composition of C101 immediately

View Article Online
DOI: 10.1039/D5RE00536A

after synthesis.[7] Since no phosphane oxides were identified at this stage, their formation must occur during the aging of the solution. Given the limited availability of phosphanes for autoxidation, the only viable alternative source are the trialkylphosphonium chloride species.

Besides the difficulty of dispersing air through the ionic liquid due to its high viscosity which hinders mass transfer, further kinetic stabilization can be linked with the presence of the acid/base equilibrium between trialkylphosphane and its corresponding trialkylphosphonium chloride species. Notably, both the protonated as well as the deprotonated form can be observed in the NMR spectrum, even in protic solvents, indicating the slow exchange.

In addition to the major variations in chemical composition, the phosphane oxide resonances exhibit substantial chemical shift differences as well, whereas other species display only minor shifts. These minor shifts can be attributed to the compositional differences of C101 across batches, but they do not account for the more significant shifts observed for the phosphane oxide signals. This behavior can be linked to the acid–base equilibrium of the P=O functional group (*vide supra*). The absence of two distinct resonances for the protonated and unprotonated form of the phosphane oxides also illustrates the faster exchange compared to the phosphane equilibrium.

The overall purity of the different batches is notable as well. Although legacy batches boasted 97.7% purity and many vendors still advertise ≥95%, the shift to a ≥93% specification more accurately represents the tetraalkylphosphonium chloride content in the commercial product. On the other hand, including the protonated phosphanes towards the products overall purity is problematic as progressive oxidation of trihexylphosphonium chloride and other minor trialkylphosphonium chloride by-products during storage renders the purity dependent on sample age and handling (*e.g.*, agitation due to transport). Nevertheless, as no information is

View Article Online
DOI: 10.1039/D5RE00536A

usually disclosed about subtle changes in the production process, it is unknown if newer batches do consistently achieve the ≥95% target.

Based on these findings, the major differences in the purification efficiencies of different batches of C101 observed by Deferm *et al.* can now be understood better.[38] Moreover, the inefficiency of the method can be linked with the neutralization step in the purification protocol which induces deprotonation of the trialkylphosphonium chloride species, converting them into their more reactive phosphane form. Although these species are expected to be more readily extracted by heptane compared to their protonated form, these phosphanes readily oxidize upon exposure to atmospheric oxygen (*vide infra*), forming additional phosphane oxides, whose removal from $[P_{66614}]^+Cl^-$ represents the primary challenge in the purification process.

Purification of C101

Purifying ionic liquids on a large scale presents significant challenges. While washing, evaporation, and crystallization are the standard industrial methods, the latter two are unsuitable for C101. Crystallization is not a viable option because the ionic liquid does not exhibit a distinct melting point, but rather vitrifies at -69.8 °C. Similarly, evaporation is not viable for the removal of high boiling-point impurities due to $[P_{66614}]^+Cl^-$ limited thermal stability.[38] Consequently, liquid–liquid extraction remains the only feasible alternative.

A recent study revealed a tenfold overestimation of the solubility of C101 in ethylene glycol solution based on phosphorus quantification by ICP-OES.[22] This overestimation was attributed to the preferential dissolution of impurities, effectively purifying C101 in the process. Consequently, this NASX approach may serve as a viable purification method for C101. To determine suitable solvent extraction conditions, phase disengagement times were

View Article Online
DOI: 10.1039/D5RE00536A

assessed for 15 combinations of temperature (21, 40, and 60 °C) and NaCl concentration (0, 0.2, 0.4, 0.6, and 0.8 mol·L^{-1}; Figure 14). Data for 0 mol·L^{-1} NaCl (pure ethylene glycol) were omitted because of severe issues with the phase disengagement, with disengagement times longer than 10 minutes. Temperature was identified as the dominant factor influencing phase disengagement, while salt concentration had a smaller effect. Based on these findings, purifications were carried out at 60 °C with ethylene glycol containing 0.2 mol·L^{-1} NaCl.

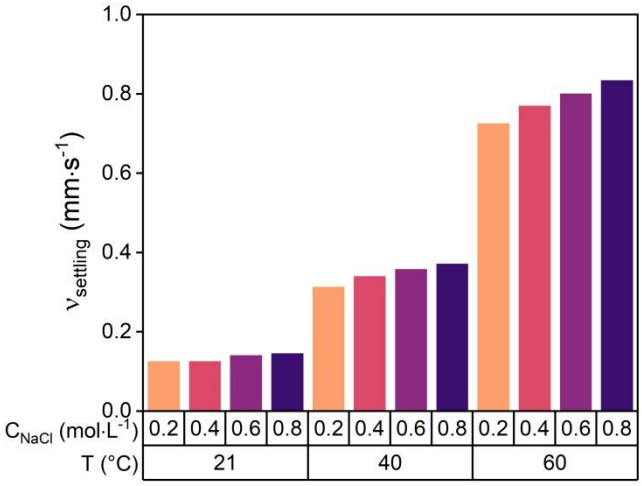

Figure 14. Settling rates as a function of temperature and NaCl concentration (Batch 2).

Because phosphanes are essentially nonpolar, ethylene glycol cannot extract them preferentially over $[P_{66614}]^+Cl^-$, as confirmed by our previous study.[22] Although apolar solvents such as heptane could, in principle, dissolve phosphanes more effectively, their concentrations in C101 are both very low and highly variable due to solution aging. Moreover, phosphane extraction would require oxygen-free conditions before and during separation, introducing unnecessary complexity for minimal benefit. Therefore, residual phosphanes were oxidized *in situ* to their corresponding phosphane oxides and phosphinates by sparging ambient air through the solution using a glass frit.

View Article Online
DOI: 10.1039/D5RE00536A

Sparging ambient air directly into neat C101 proved highly inefficient because its high viscosity prevented effective gas dispersion. To overcome this issue, C101 was first saturated with ethylene glycol, which led to a substantial reduction in viscosity and which enabled an efficient dispersion. Under these conditions, all residual phosphanes were almost instantly oxidized, as evidenced by the disappearance of their ^{31}P NMR signals after only 20 seconds at an air flow rate of 100 mL·min^{-1}. This fast oxidation highlights the strong tendency of phosphanes to be oxidized, while no observable change in the trialkylphosphonium chloride content was detected.

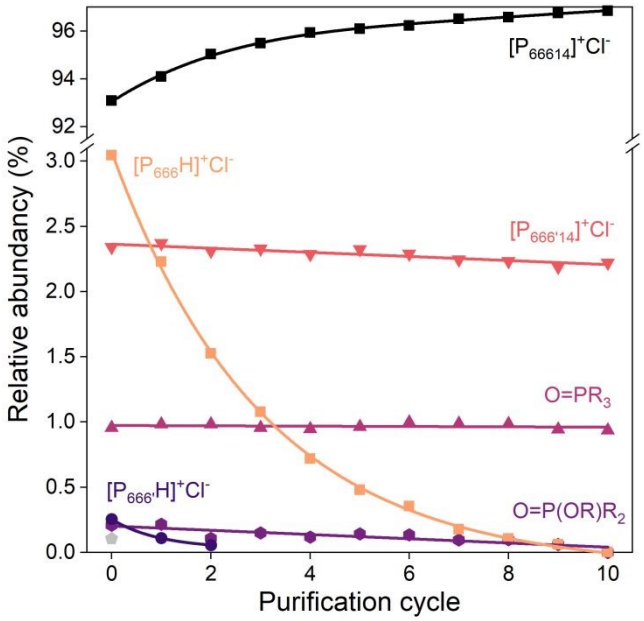

Figure 15. Relative abundance of trihexyltetradecylphosphonium chloride ($[P_{66614}]^+Cl^-$), hexan-2-yldihexyltetradecylphosphonium chloride ($[P_{666'14}]^+Cl^-$), trihexylphosphonium chloride ($[P_{666}H]^+Cl^-$), hexan-2-yldihexylphosphonium chloride ($[P_{666'}H]^+Cl^-$), trialkylphosphanes oxides ($O=PR_3$), and hexyldihexylphosphinate ($O=P(OR)R_2$) in each stage of the purification process. The grey pentagon in the left bottom corner represents the longer

View Article Online
DOI: 10.1039/D5RE00536A

homologues of $[P_{666}H]^+Cl^-$, present in low amounts and only reliably observed in the feed solution (Batch 2).

After oxidation, a 10-step batch extraction was performed using neat ethylene glycol at each stage. qNMR analysis confirmed that trihexylphosphonium chloride and its hexan-2-yl isomer were readily removed (Figure 15; SI, Figure S22). The resonance at 8.98 ppm, assigned to dodecyldihexylphosphonium chloride and tetradecyldihexylphosphonium chloride, was observed only in the feed solution and disappeared into the spectral noise after the first contact. Although qNMR effectively tracks trihexylphosphonium chloride and hexan-2-yldihexylphosphonium chloride during purification, its sensitivity is inherently limited by the signal-to-noise ratio achievable with NMR measurements.

To complement the NMR data, LC–MS analysis was performed at each purification stage. Because none of the species exhibited absorption bands in the UV-VIS-NIR spectrum between 190 and 800 nm, interpretation relied exclusively on MS signals. While MS responses are not strictly linear with concentration, relative peak areas can provide valuable insight into the extraction behavior of minor species across stages. qNMR and LC–MS show similar trends for trihexylphosphonium chloride. After 10 extraction cycles, the $[M]^+$ signal approaches baseline, indicating only trace residuals (Figure 16). A similar trend is observed for dodecyldihexylphosphonium chloride (m/z = 371.3) and dihexyltetradecylphosphonium chloride (m/z = 399.5), although both display lower apparent extractability than the main trihexylphosphonium chloride species, consistent with their longer alkyl chains (Figure 17). Despite this, both species are quantitatively removed from C101 owing to their low initial concentrations. Notably, the signal for dodecyldihexylphosphonium chloride falls below the detection limit after only 5 cycles. These results confirm that all protonated phosphanes can

View Article Online
DOI: 10.1039/D5RE00536A

be quantitatively removed from C101 with relative ease using the described multistep extraction protocol.

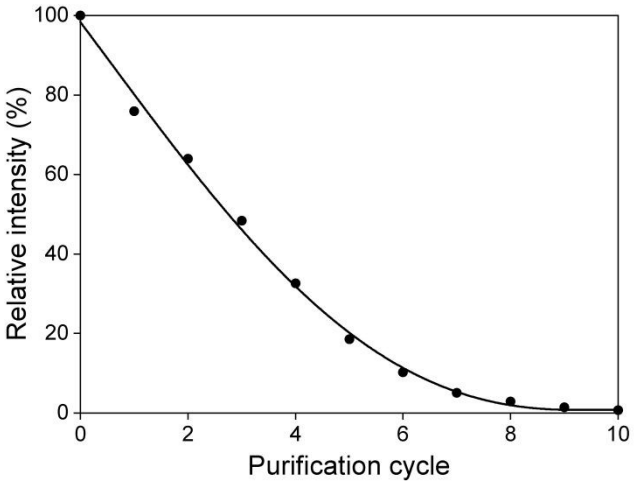

Figure 16. Relative intensity of the trihexylphosphonium chloride signal during 10 purification cycles based on LC-MS analysis (Batch 2).

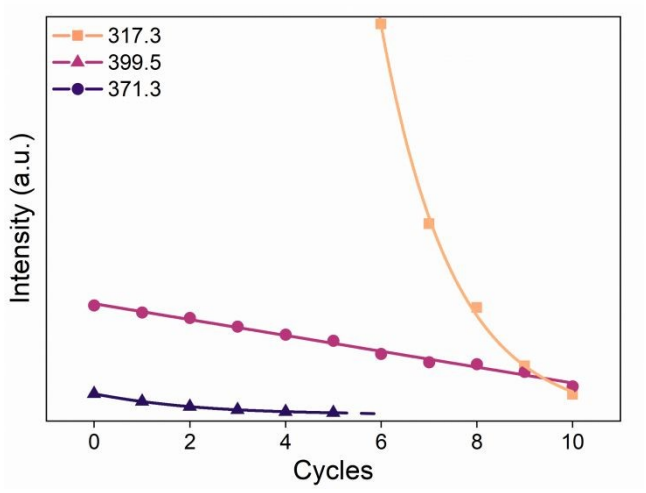

Figure 17. Absolute intensities of trihexylphosphonium chloride, dodecyldihexylphosphonium chloride, and dihexyltetradecylphosphonium chloride during 10 purification cycles based on LC-MS analysis (Batch 2).

View Article Online
DOI: 10.1039/D5RE00536A

Phosphane oxide impurities, by contrast, are far less amenable to extraction, showing negligible reductions in relative abundance throughout the purification stages. This is in stark contrast to previously reported results, which described a 3.6% reduction in phosphane oxides after ten contacts with ethylene glycol.[22] In that case, however, the starting C101 solution contained substantially larger quantities of phosphane oxides and no protonated phosphanes, indicating that much more autoxidation had occurred in the solution.

A second discrepancy is found between NMR and MS results. Based on MS alone, where the signal intensity dropped by approximately 50% (Figure 18), one might conclude extraction of both dihexyl- and trihexylphosphane oxide, whereas the increase for their longer analogues would indicate enrichment upon cycling. Although no signal (even qualitatively) is observed for dihexylphosphane oxide after purification, consistent with the MS trend, the discrepancy for trihexylphosphane oxide is particularly pronounced. This divergence highlights a limitation of the obtained MS data. The signal intensity depends on multiple factors besides concentration alone. Because phosphane oxides are partially protonated in solution, their ESI response is inherently higher. Progressive HCl extraction by ethylene glycol shifts the equilibrium toward the non-protonated oxides, suppressing MS signal without a proportional decrease in concentration. This interpretation is supported by the upfield shift of the trihexylphosphane oxide resonance after each cycle (Figure 19; SI, Figure S23). Despite this limitation for the MS data, the increasing MS signal for the longer homologues can only be accounted for by an increase in their relative abundance. This observation aligns with solubility expectations, as the main trihexylphosphane oxide exhibits a solubility nearly identical to that of $[P_{66614}]^+Cl^-$, while increasing the alkyl chain length reduces solubility.

View Article Online
DOI: 10.1039/D5RE00536A

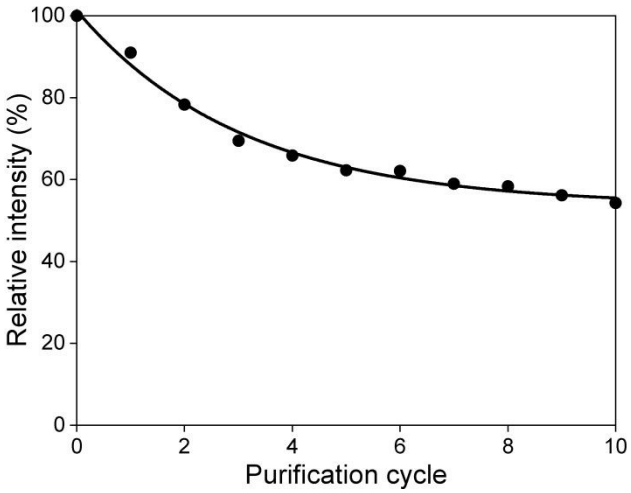

Figure 18. Relative signal intensity of trihexylphosphane oxide during 10 purification cycles based on LC-MS analysis (Batch 2).

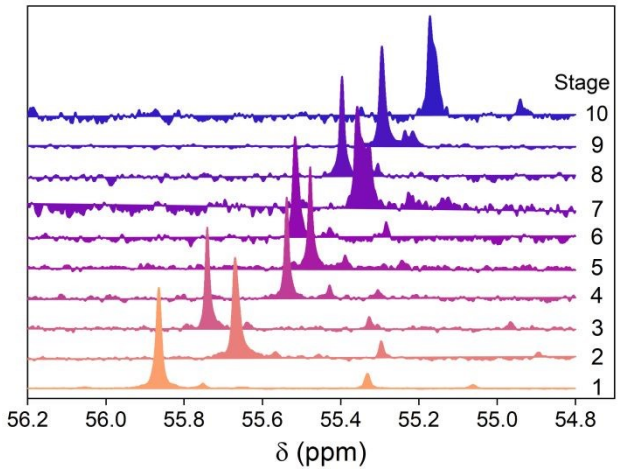

Figure 19. $^{31}P\{^{1}H\}$ NMR spectra of trihexylphosphane oxide in C101 solution at each purification stage. Conditions: 200 µL of C101, 250 µL of MeOH; internal reference: 5 wt% H_3PO_4 in D_2O (Batch 2).

The larger extent of phosphane oxide extraction reported previously can also be rationalized by protonation, since in their protonated form these species are more polar and therefore more

View Article Online
DOI: 10.1039/D5RE00536A

soluble in ethylene glycol. Therefore, its extraction not only relies on its concentration but also on the extent of free acid as well, able to form the more protonated species with and plateaus as a result of limited HCl content left after several contacts.

Similar behavior is observed for dihexylphosphane oxide (SI, Figure S24), although its decline in extraction efficiency with each stage is less pronounced than for the trihexyl analogue and does not plateau over the examined contacts.

The tetraalkylphosphonium species allow a more straightforward interpretation. Because these ions are permanently charged, their ESI response is much less sensitive changes in the solution and therefore more reflective of concentration. As expected, shorter-chain homologues show greater solubility in ethylene glycol, whereas longer-chain analogues are less soluble (Figure 20). Intriguingly, the hexyl variants appear slightly more soluble. Although the overall extraction of these ions is limited, their presence in C101 is far less problematic than that of protonated phosphanes or phosphane oxides. While they may slightly influence bulk properties such as viscosity and density, they are unlikely to participate in side reactions and exhibit electrochemical windows that are very similar to that of pure $[P_{66614}]^+Cl^-$. However, in the case of its use as an extractant, the presence of the hexan-2-yl isomer may exert a more pronounced effect on extraction behavior through altered packing around extractable metal complex. Nevertheless, its removal is neither economically justified nor required for solvent-extraction applications, particularly at larger scale, but might introduce deviations in fundamental speciation studies.

View Article Online
DOI: 10.1039/D5RE00536A

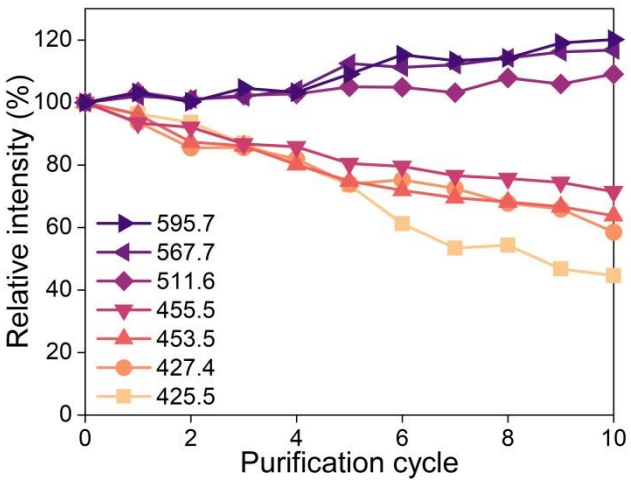

Figure 20. Relative signal intensity of the tetraalkylphosphonium chloride species during 10 purification cycles based on LC-MS analysis (Batch 2).

Column purification on mini-pilot scale

In solvent extraction research, continuous flow setups, such as mixer-settlers, centrifugal contactors, or agitated columns, are a crucial step in between initial batch scale experiments and pilot-scale trials. These setups for continuous experiments require substantially larger volumes of extractant compared to their batch counterparts. Accordingly, the described purification was extended to a proof-of-principle continuous flow setup able to purify C101 at liter scale. As the batch-scale experiments indicated the need for at least ten steps to achieve 99% tetraalkylphosphonium chlorides, an agitated column was selected because it can accommodate many theoretical stages within a compact unit, whereas mixer-settlers become particularly cumbersome when large numbers of stages are required.[56]

View Article Online
DOI: 10.1039/D5RE00536A

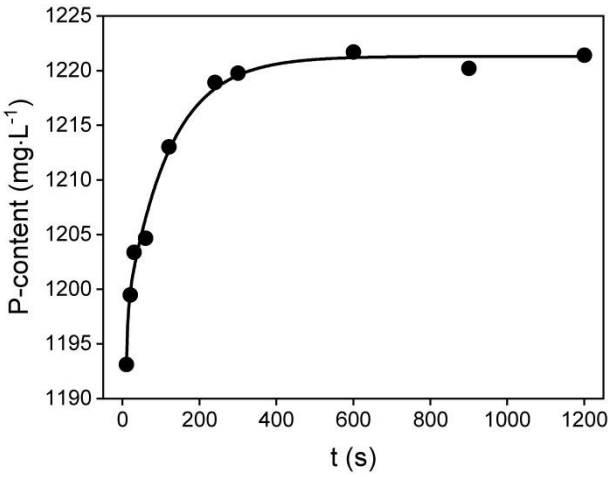

Figure 21. Amount of the dissolved phosphorus-based species as a function of time (Batch 2).

Before working in continuous flow, the kinetics of C101 purification with ethylene glycol solution was evaluated by measuring the phosphorus content in ethylene glycol after contact with C101 at different time intervals (10 – 1200 s, Figure 21). Although equilibrium was reached only after approximately 10 min, 97.5% and 99% of the equilibrium concentration were attained within 10 and 70 s, respectively. With such kinetic behavior, no major kinetic limitations are anticipated in a continuous-flow setup, and the process should perform well even at reduced residence times.

Table 3. Physical properties of both phases during solvent extraction.

Stream	ρ (g·mL^{-1})	η (mPa·s)	$v_{settling}$ (mm·s^{-1})	T (°C)	Phase continuity
Saturated C101	0.9269†	20.1†	0.72†	60	Ethylene glycol
EG + 0.2 M NaCl	1.0913	5.29			

†Determined using batch 2

The continuous extraction was carried out in a rotary agitated Kühni column connected with two preheaters to heat the original solution until 60 ± 0.5 °C before being pumped in the

View Article Online
DOI: 10.1039/D5RE00536A

temperature-controlled column, as this temperature ensures sufficient settling rates to prevent flooding (*vide supra*). The viscosity, density, and settling velocity at the chosen conditions are summarized in Table 3. Initially, both the more polar and less polar phases were pumped at 50 $mL \cdot min^{-1}$ with a stirring speed of 300 rpm. Within the first 90 min of operation, flooding was detected visually by periodic sampling every 20 min. To alleviate this, the flow rates of both phases were systematically reduced from 50 $mL \cdot min^{-1}$ to 38 $mL \cdot min^{-1}$ while the stirring speed was lowered to 200 rpm. After these adjustments, the column gained a stable dispersion, and no further flooding was observed. Any operation above these flow rates and stirring speeds consistently renewed flooding, indicating that these conditions represent the upper operational composition. Following the initial parameter correction, a steady state was achieved after approximately 200 min, as evidenced by the constant outlet composition (Figure 22). Analysis of the extracted product revealed a final purity of 99.0% (based on the total tetraalkylphosphonium chloride content), matching the purity obtained in the batch extraction experiments (SI, table S2).

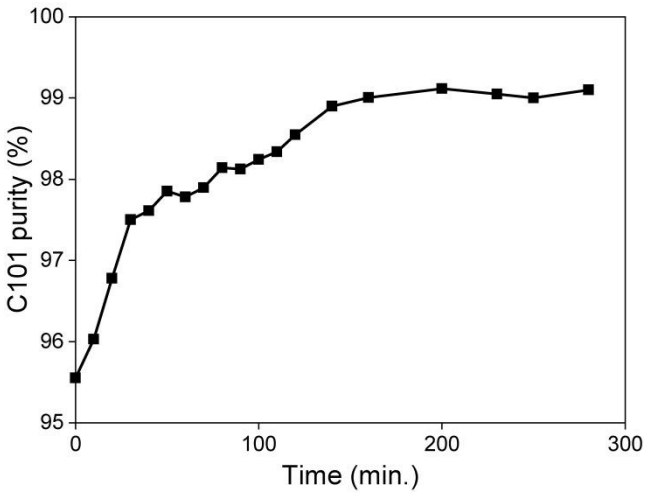

Figure 22. Tetraalkylphosphonium chloride content in C101 as a function of time during the counter-current solvent extraction experiment (Batch 2).

View Article Online
DOI: 10.1039/D5RE00536A

Conceptual flowsheet

Based on the current results, a conceptual flowsheet for the continuous purification of C101 is shown in Figure 23. The neat C101 is first contacted with ethylene glycol and NaCl to presaturate the C101 phase, thereby preventing volumetric fluctuations between the inlet and outlet streams of the agitated extraction column. The presaturated C101 solution is fed directly into the agitated column for impurity removal using an ethylene glycol solution with 0.2 $mol \cdot L^{-1}$ NaCl. A dedicated oxidation step for residual phosphane oxides is omitted. The small amount of non-protonated phosphanes present readily oxidize during the presaturation step if conducted under ambient atmosphere, making an additional oxidation stage unnecessary, as evidenced by the absence of any phosphane signal in the NMR spectra after presaturation. Following purification, the ethylene glycol and NaCl dissolved in C101 must be removed. This can be achieved by washing the C101 solution with water. Afterwards the purified C101, now saturated with water, can be dried by distillation. The purified solution is obtained, and the removed water can be recycled for the washing step. On the other hand, the mixture of water, ethylene glycol and small amounts of sodium chloride from the washing step can be recycled using distillation and subsequently reused for the saturation step and washing step, although salt effects on distillation behavior should be considered and further investigated. Moreover, the method remains dependent on the initial batch composition to be treated, as phosphane oxides remain problematic to remove. Therefore, purification is best performed immediately after synthesis, or at least before significant conversion of the readily extractable trialkylphosphonium chlorides into more problematic phosphine oxides occurs.

View Article Online
DOI: 10.1039/D5RE00536A

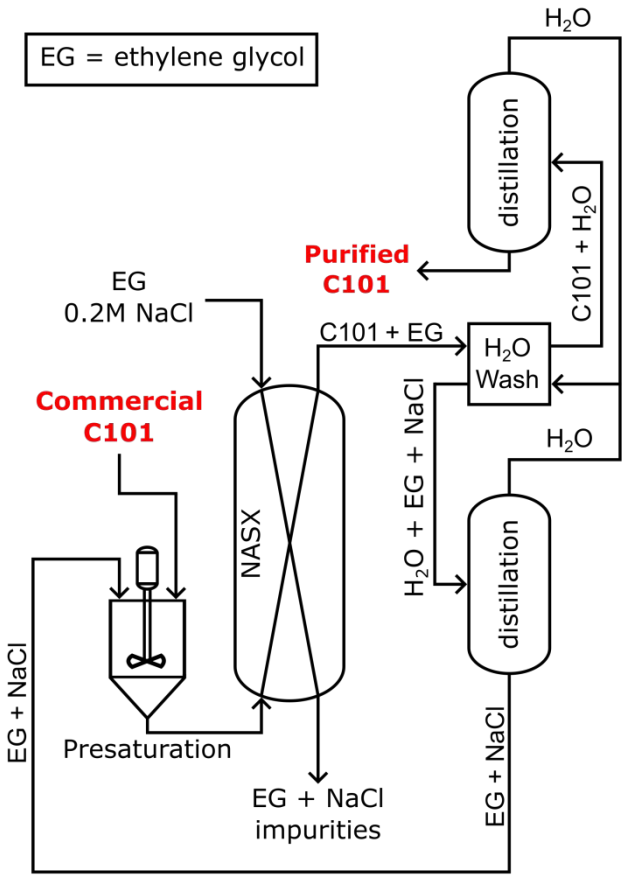

Figure 23. Conceptual flowsheet for the purification of C101 by NASX using ethylene glycol and sodium chloride.

View Article Online
DOI: 10.1039/D5RE00536A

Conclusions

In this work, the chemical complexity of the commercial quaternary phosphonium ionic liquid Cyphos IL 101 was characterized using ^{31}P NMR and LC–MS analysis. At least 22 distinct phosphorus-containing species were identified in the commercial compounds, revealing a far greater diversity than is generally assumed.

The importance of protic solvents for the measurement of NMR, particularly in the case of quantification, is demonstrated. The major broadened signal of the phosphane oxides, often causing the inability for the signal to be detected, was determined to be caused by sever exchange broadening as a result of proton exchange. The use of alternative solvents, such as methanol, or the addition of ethylene glycol, proved to reliably solve this issue by increasing the exchange rate compared to the non-protic chloroform solvent.

Substantial batch-to-batch variations was also uncovered, particularly in the relative abundance of phosphane oxides and protonated phosphanes. These differences appears tied to the product's aging, governed by the gradual autoxidation of phosphane species during storage and handling.

A purification strategy using ethylene glycol containing NaCl was developed. This protocol proved capable of removing all trialkylphosphonium chlorides quantitatively. However, the method exhibited limited efficiency in removing phosphane oxide impurities, most likely linked with the lack of protonation, indicating the importance of timely processing or controlled handling conditions during storage.

Finally, a mini-pilot purification approach is illustrated with a counter-current agitated column. This setup enabled liter-scale purification of Cyphos IL 101 under continuous-flow conditions, validating the feasibility of scale-up. Based on these results, a conceptual flowsheet for the continuous purification of Cyphos IL 101 is presented.

View Article Online
DOI: 10.1039/D5RE00536A

The significant fluctuations in the chemical composition of Cyphos IL 101 between batches and within a single batch over time, can have serious negative consequences for its usefulness and similar quaternary phosphonium salts as basic extractants for metal ions. This issue arises in addition to the already recognized challenges associated with ionic liquids, such as their relatively high cost and limited recyclability. Since several of the impurities present in the commercial ionic liquid might behave as extractants themselves, it is very difficult to predict the extraction behavior of Cyphos IL 101 *a priori*, and the extraction performance is also expected to change over time as a result of the autoxidation of some these impurities. The compositional variation of Cyphos IL 101 can also provide a possible explanation for some conflicting solvent extraction results that have been reported in the literature for this compound. However, the exact effect of all impurities on metal solvent extraction systems cannot be fully assessed yet, as the current method remains unable to deal with the phosphane oxides. This variation in chemical composition is not observed for the main alternative basic extractant, the quaternary ammonium salt Aliquat 336. Colleagues working with Cyphos IL 101 as an extractant are advised to purify the material prior to use, synthesize it via alternative routes, or thoroughly document its exact composition. In addition, tracking batch numbers is strongly recommended.

Supplementary Information

View Article Online
DOI: 10.1039/D5RE00536A

Supplementary data to this article can be found online at …

Acknowledgements

The authors would like to thank the Research Foundation-Flanders (FWO Flanders) for the financial support through research grant G0D7421N, infrastructure grant I002720N, and infrastructure grant I001920N. Jakob Bussé is gratefully acknowledged for his aid with the development of the preheating system for the extraction column setup. Dr. Nand Peeters is acknowledged for his aid with the counter-current column experiment. Dr. Clio Deferm is acknowledged for sharing her experience with purification of Cyphos IL 101. Dr. Gert Steurs is acknowledged for his aid in measuring the T_1 delay times. Bart Van Huffel is acknowledged for his aid with the LC-MS measurements.

Conflict of interest

There are no conflicts to declare.

View Article Online
DOI: 10.1039/D5RE00536A

References

1 T. Welton, *Chem. Rev.*, 1999, **99**, 2071–2084.

2 J. P. Hallett and T. Welton, *Chem. Rev.*, 2011, **111**, 3508–3576.

3 J. D. Holbrey and K. R. Seddon, *Clean Technol. Environ. Policy*, 1999, **1**, 223–236.

4 N. V. Plechkova and K. R. Seddon, *Chem. Soc. Rev.*, 2008, **37**, 123–150.

5 A. J. Greer, J. Jacquemin and C. Hardacre, *Molecules*, 2020, **25**, 5207.

6 K. Binnemans and P. T. Jones, *Journal of Sustainable Metallurgy*, 2023, **9**, 423–438.

7 C. J. Bradaric, A. Downard, C. Kennedy, A. J. Robertson and Y. Zhou, *Green Chem.*, 2003, **5**, 143–152.

8 K. J. Fraser and D. R. MacFarlane, *Aust. J. Chem.*, 2009, **62**, 309–321.

9 S. Wellens, B. Thijs and K. Binnemans, *Green Chem.*, 2012, **14**, 1657–1665.

10 S. Wellens, R. Goovaerts, C. Möller, J. Luyten, B. Thijs and K. Binnemans, *Green Chem.*, 2013, **15**, 3160–3164.

11 T. Vander Hoogerstraete, S. Wellens, K. Verachtert and K. Binnemans, *Green Chem.*, 2013, **15**, 919–927.

12 M. Rzelewska-Piekut and M. Regel-Rosocka, *Sep. Purif. Technol.*, 2019, **212**, 791–801.

13 M. Regel-Rosocka and M. Wisniewski, *Hydrometallurgy*, 2011, **110**, 85–90.

14 L. Cui, F. Cheng and J. Zhou, *Ind. Eng. Chem. Res.*, 2015, **54**, 7534–7542.

15 L. Xu, C. Chen and M. L. Fu, *Hydrometallurgy*, 2020, **197**, 105439.

16 K. Pianowska, J. Kluczka, G. Benke, K. Goc, J. Malarz and K. Leszczyńska-Sejda, *Sci. Rep.*, 2024, **14**, 17806.

17 Ş. Sert and S. Yusan, *J. Radioanal. Nucl. Chem.*, 2023, **332**, 2601–2611.

18 Z. Abbas and S. M. Jung, *ACS Omega*, 2024, **9**, 44304–44311.

19 C. Deferm, B. Onghena, T. Vander Hoogerstraete, D. Banerjee, J. Luyten, H. Oosterhof, J. Fransaer and K. Binnemans, *Dalton Trans.*, 2017, **46**, 4412–4421.

20 Z. Zhu, P. Yoko and C. Y. Cheng, *Hydrometallurgy*, 2017, **169**, 213–218.

21 C. Deferm, B. Onghena, V. T. Nguyen, D. Banerjee, J. Fransaer and K. Binnemans, *RSC Adv.*, 2020, **10**, 24595–24612.

22 V. Cool, S. Riaño, T. Van Gerven and K. Binnemans, *Sep. Purif. Technol.*, 2024, **333**, 125787.

23 M. L. P. Reddy, R. L. Varma, T. R. Ramamohan, S. K. Sahu and V. Chakravortty, *Solvent Extr. Ion Exch.*, 1998, **16**, 795–812.

24 H. Tong, D. Li, Y. Wang and J. Lei, *Wuhan Univ. J. Nat. Sci.*, 2003, **8**, 871–874.

25 T. Sato, *J. Radioanal. Nucl. Chem.*, 1986, **101**, 77–114.

26 O. Kuzmina and J. P. Hallett, *Application, Purification, and Recovery of Ionic Liquids*, Elsevier, 2016.

27 P. Wasserscheid and T. Welton, *Ionic Liquids in Synthesis*, Wiley, 2007.

28 B. Clare, A. Sirwardana and D. R. MacFarlane, in *Ionic Liquids*, ed. B. Kirchner, Springer, Heidelberg, 2009, vol. 290, pp. 1–40.

29 P. Nockemann, K. Binnemans and K. Driesen, *Chem. Phys. Lett.*, 2005, **415**, 131–136.

30 K. R. Seddon, A. Stark and M.-J. Torres, *Pure Appl. Chem.*, 2000, **72**, 2275–2287.

31 J. Zhou, H. Sui, Z. Jia, Z. Yang, L. He and X. Li, *RSC Adv.*, 2018, **8**, 32832–32864.

32 S. Santasalo and S. K. Wiedmer, *J. Chromatogr. Open*, 2025, **8**, 100239.

33 M. J. Earle, C. M. Gordon, N. V. Plechkova, K. R. Seddon and T. Welton, *Anal. Chem.*, 2007, **79**, 758–764.

34 A. K. Burrell, R. E. Del Sesto, S. N. Baker, T. M. McCleskey and G. A. Baker, *Green Chem.*, 2007, **9**, 449–454.

35 N. Srivastava, M. Shukla and S. Saha, *Indian J. Chem.*, 2010, **49A**, 757–761.

36 J. Zhou, H. Sui, Z. Jia, Z. Yang, L. He and X. Li, *RSC Adv.*, 2018, **8**, 32832–32864.

37 M. J. Earle, J. M. S. S. Esperança, M. A. Gilea, J. N. Canongia Lopes, L. P. N. Rebelo, J. W. Magee, K. R. Seddon and J. A. Widegren, *Nature*, 2006, **439**, 831–834.

38 C. Deferm, A. Van Den Bossche, J. Luyten, H. Oosterhof, J. Fransaer and K. Binnemans, *Phys. Chem. Chem. Phys.*, 2018, **20**, 2444–2456.

39 A. R. Choudhury, N. Winterton, A. Steiner, A. I. Cooper and K. A. Johnson, *CrystEngComm*, 2006, **8**, 742–745.

40 J. T. Hamill, C. Hardacre, M. Nieuwenhuyzen, K. R. Seddon, S. A. Thompson and B. Ellis, *Chem. Commun.*, 2000, 1929–1930.

41 J. Bartosik and A.-V. Mudring, *Phys. Chem. Chem. Phys.*, 2010, **12**, 4005–4011.

42 D. S. Choi, D. W. Choi, E. J. Park, S. K. Chang, I. S. Byun and W. J. Kim, WO 2004/080974 A1, 2004.

43 M. G. Bogdanov and I. Svinyarov, *Sep. Purif. Technol.*, 2018, **196**, 57–60.

View Article Online
DOI: 10.1039/D5RE00536A

44 C. Deferm, *Personal Communication*, 2024.

45 K. D. Troev, in *Reactivity of P-H Group of Phosphorus Based Compounds*, Elsevier, 2018, pp. 19–144.

46 S. A. Buckler, *J. Am. Chem. Soc.*, 1962, **84**, 3093–3097.

47 L. McEwan, *Selective Catalytic Hydrogenation for Industrial 1-Hexene Purification*, Master's Thesis, University of Cape Town, 2010.

48 L. McEwan, M. Julius, S. Roberts and J. C. Q. Fletcher, *Gold Bull.*, 2010, **43**, 298–306.

49 B. Onghena, S. Valgaeren, T. Vander Hoogerstraete and K. Binnemans, *RSC Adv.*, 2017, **7**, 35992–35999.

50 O. Kühl, *Phosphorus-31 NMR Spectroscopy*, Springer Berlin Heidelberg, Berlin, Heidelberg, 2009.

51 J. Keeler, *Understanding NMR Spectroscopy*, Wiley, 2nd edn., 2012.

52 C. J. Jameson and H. J. Osten, in *Annual Reports on NMR Spectroscopy*, ed. Webb G. A., Academic Press, 1986, vol. 17, pp. 1–78.

53 D. G. Gorenstein, *Phosphorus-31 NMR : principles and applications*, Academic Press, 1984.

54 J. C. Tebby, *Handbook of Phosphorus-31 Nuclear Magnetic Resonance Data*, CRC Press, Boca Raton, 1st edn., 2017.

55 L. D. Quin and A. J. Williams, *Practical Interpretation of P-31 NMR Spectra and Computer Assisted Structure Verification*, Advanced Chemistry Development, Toronto, 2004.

56 I. R. Rodrigues, C. Deferm, K. Binnemans and S. Riaño, *Sep. Purif. Technol.*, 2022, **296**, 121326.

View Article Online
DOI: 10.1039/D5RE00536A

Data availability statement

View Article Online
DOI: 10.1039/D5RE00536A

The data supporting this article have been included as part of the Supplementary Information.